Nanoscale

PAPER

View Article Online
View Journal | View Issue

Cite this: *Nanoscale*, 2023, **15**, 15982

Ultra-light-weight microwave X-band EMI shielding or RAM material made from sustainable pyrolysed cork templates

Robert C. Pullar, *[a] Rui M. Novais,[b] Ana. P. F. Caetano,[b] K. A. Krishnakumar[c] and Kuzhichalil P. Surendran [c]

Received 1st September 2023,
Accepted 28th September 2023

DOI: 10.1039/d3nr04411d

rsc.li/nanoscale

Cork is a renewable and sustainable material, highly porous and lightweight. We valorised waste cork and recycled wine stoppers to make pyrolysed/carbonised solid cork, for use as economic and sustainable microwave (MW) absorbers at the microwave X-band (8–12 GHz), without binder or additives. Although cork is already a very lightweight material (0.16 g cm^{-3}), the pyrolysed cork is five-times less dense at 0.031 g cm^{-3}, was amorphous graphitic carbon, and had an excellent shielding effectiveness (SE_T) of −18 to −38 dB, depending on thickness, with attenuation of the electromagnetic energy through internal reflection within the cellular cork structure. Furthermore, this ultra-light-weight material has an extremely high MW specific shielding effectiveness or efficiency (SSE), between −640 to −1235 dB g^{-1} cm^3 over the entire X-band range, depending on thickness (3.0–8.6 mm), one of the highest reported for any pure carbon material, this upper value being more than twice that of any previously reported graphite-based foams.

1. Introduction

Cork is the bark of a Mediterranean evergreen oak tree (*Quercus suber* L.), with around 50% being supplied by Portugal,[1] the world's largest cork producer.[2] Cork is a uniquely sustainable resource as it is harvested from the tree every 9–12 years,[3] without damaging the tree, which has an active productive life of at least 200 years (~20 harvests). It is renewable, since the cork layer is regenerated after each extraction, and will absorb the equivalent amount of CO_2 which may be released from the cork during processing; hence, cork extraction actually increases the CO_2 absorption of the tree during its lifetime by up to five times,[4] and cork can sequester up to 5.7 T CO_2 per ha per year.[5] Furthermore, cork oak forests of Portugal are one of the best global examples of balanced conservation and development, playing a key role in ecological processes such as water retention, soil conservation and carbon storage, and supporting the greatest degree of biodiversity anywhere in Europe.[5]

Cork has a microstructure different to other lignocellulosic woods, consisting of hollow polyhedral cells, with a hexagonal honeycomb shape (~20 μm diameter) in the radial direction coming out of the tree, and a rectangular shape (~45 μm length, resembling a brick wall) in the transverse side or top directions.[5,6] The cell walls are no more than 1 μm thick. There are up to 200 million cells per cm^3,[7] giving cork a very low density of 0.12–0.24 g cm^{-3},[8] the higher densities occurring when the cell walls are corrugated. Although most woods have a density of around 0.4–0.8 g cm^{-3},[9] few are highly porous and lightweight. Even pine and bamboo are several times more-dense than cork, and only balsa (0.16 g cm^{-3}, a tropical wood sometimes called "corkwood", although it is not cork) can compare to the low density of cork, but is much less sustainable to produce as the whole tree is killed in harvesting.[10] Commercial cork is often immersed in hot water (100 °C, "boiled cork") to expand the cork cells by removing the corrugations, to give a more regular and uniform cell structure[8] with densities as low as only 0.12 g cm^{-3}.

Being 100% renewable, cork has a considerable advantage over other carbonaceous materials, contributing towards sustainable production. The most common use of cork is still as a stopper for wine bottles, and 13 billion are produced annually worldwide,[11] and tens of thousands of tonnes of wine corks are collected each year for recycling.[12] Wine corks can be made from a single solid piece of cork, agglomerated cork granules, or a composite of both. Cork powder is the main waste of the cork industry,[13] with an annual production of this waste

[a]*Dipartimento di Scienze Molecolari e Nanosistemi (DSMN), Università Ca' Foscari Venezia, Via Torino 155, 30172 Venezia Mestre, Venezia, VE, Italy.*
E-mail: robertcarlyle.pullar@unive.it
[b]*Department of Engineering of Materials and Ceramics/CICECO – Aveiro Institute of Materials, University of Aveiro, Campus Universitário de Santiago, 3810-193 Aveiro, Portugal*
[c]*Materials Science and Technology Division, CSIR-NIIST, Industrial Estate, Trivandrum 695019, India*

powder estimated at 50 000 tonnes.[14] This low economic value residue is mainly for energy generation through its combustion,[15] although the possibility of using cork waste as a precursor for activated carbon preparation *via* pyrolysis/carbonisation has been demonstrated.[14,16,17] The authors have previously reported on pyrolysed cork, both as a precursor to make biomimetic ecoceramics,[18–20] and as sustainable absorbents for pollutants in waste waters.[21]

However, this article is the first time that pyrolysed/carbonised cork has been investigated as an ultra-light-weight microwave absorber. There is a great deal of interest in materials which can absorb energy in the microwave to millimetre wave range (wavelengths of 1 m to 1 mm, frequencies of 300 MHz to 300 GHz). These have applications for EM shielding in devices and components, and electromagnetic interference (EMI) shielding and electromagnetic compatibility (EMC) testing and standards measurements, as well as in security, communications blocking, stealth technology and radar absorbing materials (RAM) for military use.[22] There are also increasing concerns about the possible negative health implications of microwaves (MW) on the human body. In the case of stealth technology, RAM coatings on aircraft, naval vessels and missiles, and portable/wearable shielding, it is particularly important to employ light-weight materials. Of particular interest is the X-band, from 8–12 GHz, used for military radar and communications, some commercial and civil wireless and satellite communications, motion sensors and speed detection devices.

Amorphous and graphitic carbon is a well-known GHz/MW absorbing material,[23] and has been used as a powder (carbon black, charcoal, graphite),[24,25] carbon fibre,[26] carbon nanotubes (CNTs),[27,28] carbon nanorods[29] and graphene.[30] However, in nearly all cases the carbon is mounted in a composite with a polymer matrix,[22] with densities of 1 g cm^{-3} or more, and there has been relatively little research into truly light-weight (density $\ll$ 1 g cm^{-3}) microwave absorbing materials.

Generally, a practical microwave absorbing material should have a shielding effectiveness (SE) of at least −10 dB, while an excellent shielding material should have a SE of at least −30 dB, throughout the frequency region to be eliminated (*e.g.*, from 8–12 GHz). However, many papers report very high values which are really only a peak value over a limited frequency range, and often choose to ignore the true values over the entire range, *e.g.* ref. 22–24, 29 and 30 Nevertheless, some authors have reported excellent absorption across the X-band with CNT-PMMA polymer composites[28] and CNT-reinforced pyrolysed carbon fibre composites.[26] Despite having high microwave attenuation, most of the composite based EM wave shields fail at the harsh environmental conditions demanded by several satellite, automotive and aeronautical applications. In this regard, high temperature durable, polymer free and light-weight EMI shields are of great technological significance.

In this paper, we report pyrolysed cork materials with similarly excellent absorption across the X-band, but also remarkably high specific shielding effectiveness, also sometimes known as specific shielding efficiency (SSE, in dB g^{-1} cm^3), due to their ultra-low density.

2. Experimental

The cork powder waste was supplied by a Portuguese cork industry (Amorim), with a stated particle size of around 200–500 μm and a density of 0.05–0.07 g cm^{-3},[31] while the used solid wine corks were supplied by the authors. This solid cork had a measured density of 0.163 g cm^{-3}.

The cork samples (powder or whole wine corks) were placed in graphite crucibles and then pyrolysed under nitrogen in a graphite furnace according to the following cycle: (i) 5 °C min^{-1} heating rate up to 150 °C; (ii) 10 °C min^{-1} heating rate up to 900 °C; 30 min dwell time at this temperature; and (iv) cooling (at 10 °C min^{-1}) to room temperature. The cork was not activated, either before or after pyrolysis. The cork microstructure was maintained in the carbon product using this heating regime.

Scanning electron microscopy (SEM) images were taken with a Hitachi S-4100 microscope, on samples coated with carbon. The crystal structure of the pyrolysed cork was assessed by X-ray diffraction (XRD), using a PANalytical X'PERT PRO 3 instrument (Cu Kα radiation, 2.5–80°, 0.01° 2θ step-scan and 200 s per step) with phase identification by HighScore Plus software. Raman spectra were taken with a Bruker RFS 100/S spectrometer using a Nd-YAG laser (1064 nm, 350 mw) on a sample mixed in a KBr disc, with 200 scans at a resolution of 4 cm^{-1}. Simultaneous thermogravimetric-differential scanning calorimetry (TG-DSC) was performed using a Setsys Evolution 1750 (Setaram), with samples being heated at 10 °C min^{-1} under nitrogen. The bulk density of solid cork, pyrolysed solid cork and cork-wax composites was measured by the geometric method.

For the microwave shielding measurements in the X-band, the studies were carried out in a vector network analyser (Agilent E5071C) using the transmission waveguide method to determine the magnitude of complex scattering parameters (S_{11} and S_{21}). From the measured scattering data, absorption shielding effectiveness (SE_A), reflection shielding effectiveness (SE_R) and total shielding effectiveness (SE_T = SE_R + SE_A) were calculated. Appropriate calibrations were carried out before the measurement, to eliminate errors due to directivity, source match, load match, isolation, *etc*. Solid cork samples were made into a rectangular block shape of 10.1 × 22.9 mm, with varying thickness, through machining using a polishing machine (Struers Tegramin-25) and fine grinding using sand-coated polishing paper. Samples with thicknesses between 3 and 8.6 mm were prepared. Cork powder samples were suspended in paraffin wax in the ratio (powder to wax) of 1 : 4 by mass. The composite was then hot pressed to form 10.1 × 22.9 mm rectangles. SSE (specific shielding effectiveness or efficiency) was calculated from

density. For comparison, we also measured un-pyrolysed cork samples.

3. Results and discussion

3.1 Pyrolysis of cork

Photographs and SEM images of the cork types used as starting materials are shown in Fig. 1. Both wine corks and waste granules were produce from boiled/expanded cork, and consisted of cells of around 15 μm diameter. The microstructure of cork is already well known, and has been characterised and discussed in detail previously.[3,7,8] Here the SEM micrographs show the regularly arranged, honeycomb like cellular structure, with their lateral cell walls randomly oriented. In the orthogonal radial direction, these honeycomb structures form rectangular/lenticular channels which could act as microwave attenuators through total internal reflection.

The TG-DSC plots of cork undergoing pyrolysis under a nitrogen atmosphere are shown in Fig. 2. The initial endothermic weight loss up to 100 °C is the loss of water, around 8 wt%. Cork is made of about 45% suberin, 27% lignin, 12% celluloses, 6% waxes and 6% tannins.[8] It is the high suberin content that enables cork to have its particular microstructure. Cellulose and lignin are broken down, releasing H_2O, CO_2 and volatile compounds, below 400 °C,[6] but suberin is more resistant, which is why cork is fire resistant to up to 500 °C.[8] Therefore, the gradual exothermic weight loss from 200 °C to 400 °C, with a DSC peak at around 350 °C, is the loss of these more volatile molecules, with a weight loss of around 30% between 100–400 °C. There is then a more sudden, weight loss of a further ~45% between 400–500 °C, after which there is no further change, which will mostly be the conversion to carbon

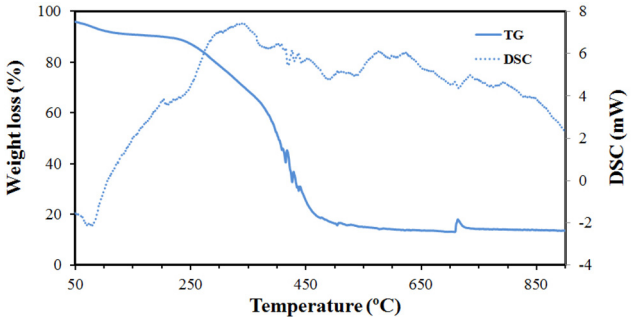

Fig. 2 TG-DSC plots of the pyrolysis of cork under nitrogen.

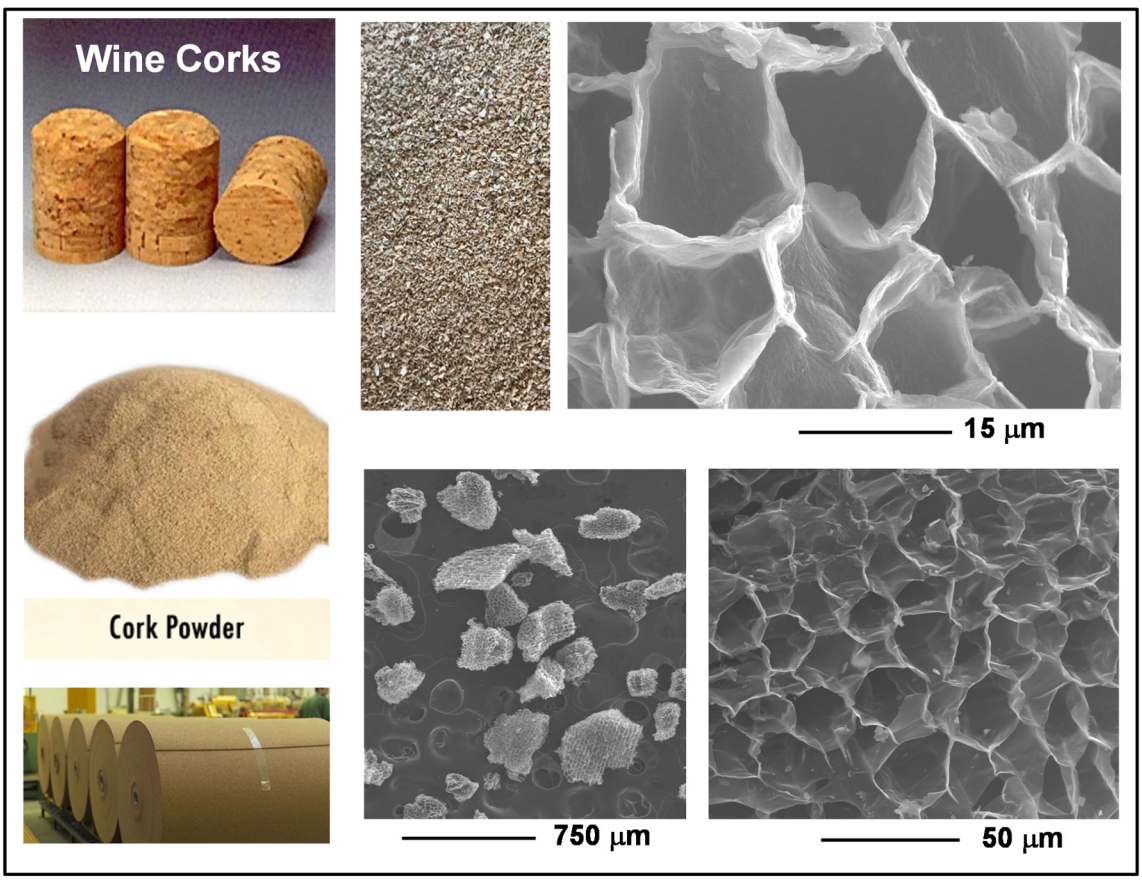

Fig. 1 Photographs of wine corks, MF5 waste cork powder and rolls of 5 mm thick cork sheets, along with SEM images of their typical microstructure.

of the remaining suberin. The total weight loss in pyrolysis is around 85%.

A photograph of solid cork before and after pyrolysis is shown in Fig. 3a. It can be seen that although the cork undergoes around 85% weight loss, it also in fact expands by 34 vol%, to give a very low volume of between 0.030–0.035 g cm^{-3} – there is some natural variation between cork samples (such as age of cork when harvested, depth within the piece of bark, seasonal growth variations, *etc.*). The solid pyrolysed cork samples measured here had a density of 0.031 g cm^{-3}. The reason for this expansion can be seen in the SEM image of pyrolysed cork in Fig. 3b. Although much weight has been lost, and the cell walls appear thinner (to as little as 200 nm wide), the walls of the cells are much straighter and have lost any remaining corrugation or un-evenness observed in the un-pyrolysed cork (Fig. 1), resulting in an increased volume. This is presumably analogous to the boiling treatment, where volatile gasses released during the pyrolysis process have had a similar, bit more extreme, effect on the microstructure.

The Raman spectrum of the pyrolysed solid cork is shown in Fig. 4a. This shows two broad peaks of roughly equal height, centred around 1600 and 1300 cm^{-1}. This is typical of amorphous or mesoporous graphitic carbon, where the G band at 1600 cm^{-1}, resulting from the C–C bond stretch in sp^2 carbon,[32] and which is a strong narrow peak in crystalline, well ordered graphite, becomes lower and broader when the carbon is disordered. This is accompanied by an increase in the size of the D band around 1300 cm^{-1}, which is induced by disorder, corresponding to very small graphitic domains and crystalline imperfections.[33] The ratio of the intensity of D : G

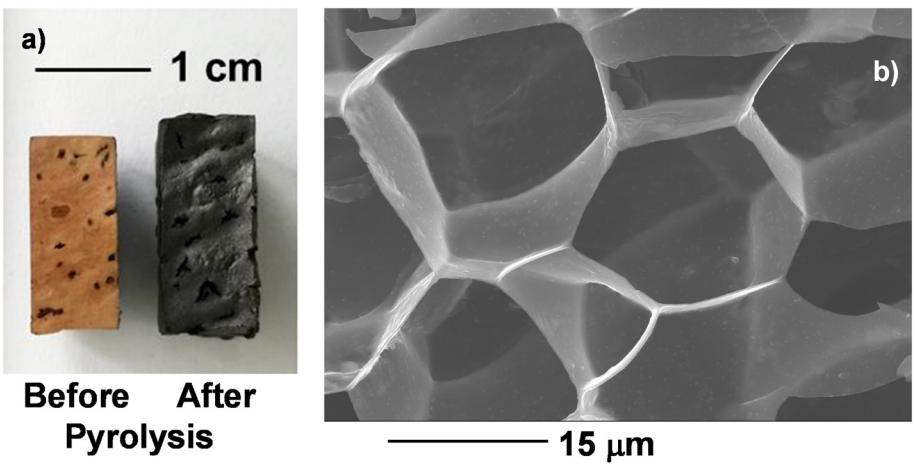

Fig. 3 (a) Photograph of solid cork before and after pyrolysis, and (b) SEM image of pyrolysed cork.

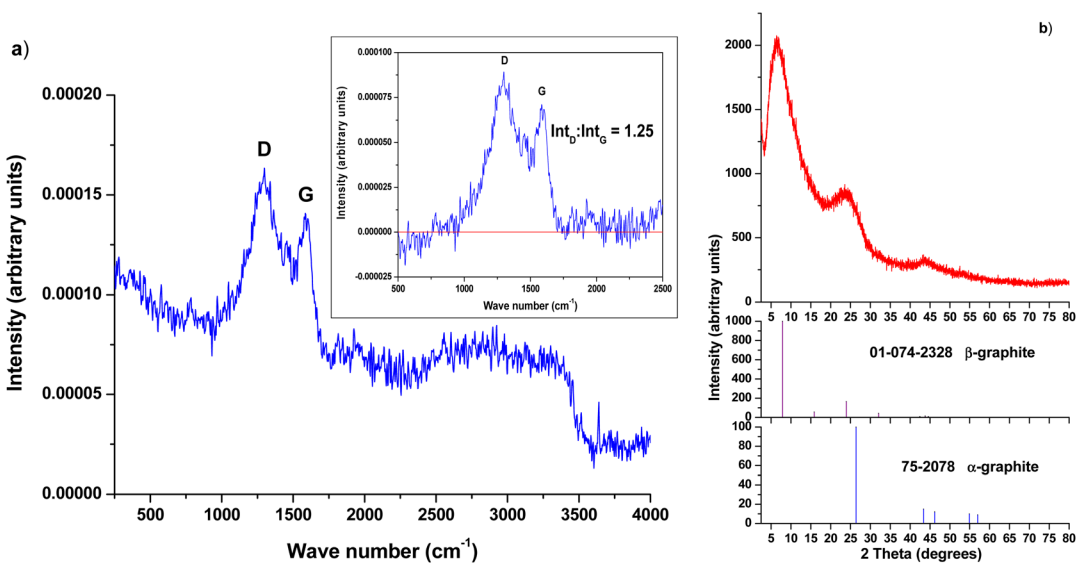

Fig. 4 (a) Raman spectrum of pyrolysed solid cork – the inset shows the relative intensities of the D and G peaks with the baseline subtracted. (b) XRD pattern of pyrolysed solid cork, with the JCPDF standards for rhombohedral β-graphite and hexagonal α-graphite.

can be seen as a degree of disorder in the carbon – in these samples the two peaks are of broadly equal intensity, indicating a highly amorphous carbon.[34] When the baseline is corrected (see inset in Fig. 4a), the actual ratio of the intensity of D : G is 1.25, indicating a highly disordered carbon structure.[35] This can also be an indication of mesoporous carbon.[36]

The nitrogen content of oak wood (cork is a type of oak) varies between around 0.2–1.1%, depending on the species and the part of the tree analysed.[37] Therefore, we would expect there to be a remaining small N content in any carbon from pyrolysed wood, and this percentage will be greater in the pyrolysed carbon than in the original wood, as O and H is lost in the process. We have shown that our cork pyrolysed in N_2 contained 1.57 wt% nitrogen,[38] which is of the levels to be expected from the original wood content, and probably does not indicate any extra N doping from the pyrolysis atmosphere. We have also previously tried argon atmospheres as well,[18] and have observed no difference in the products.

The XRD pattern of pyrolysed solid cork is shown in Fig. 4b. The main XRD peak for hexagonal crystalline graphite occurs at 2 theta = 26.4°, and is a very sharp peak in well-ordered hexagonal graphite, with a second much smaller peak at 44.3° (JCPDF 75-2078). In our samples this peak is around 24° and is quite broad and with low intensity, providing further evidence that the carbon here is poorly ordered, amorphous graphite. Interestingly, we also see a clear, large peak at 7°, which does not occur in normal, hexagonal graphite, but is attributed to rhombohedral graphite. Hexagonal graphite (α-graphite) is the most common form, being more thermodynamically stable, and synthetic graphite is usually hexagonal, with an AB lattice. However, graphite can also exist in a rhombohedral form (β-graphite, $R\bar{3}m$ (166), JCPDF 01-074-2328), with an ABC lattice, and natural biogenic graphite can consist of both structures. Rhombohedral β-graphite is thermodynamically unstable, and can be considered as an extended stacking fault of hexagonal graphite. It is never found in its pure form, but always in combination with hexagonal α-graphite, at times in up to approximately equal amounts in some natural materials.[39] It would seem to be the case that the carbon of our pyrolysed cork, a natural biogenic source, readily forms the rhombohedral β-form, although it contains hexagonal α-graphite as well, as would be expected. Although β-graphite is less thermodynamically stable, temperatures up to 1600 °C are required to transform it to the hexagonal α-graphite form, once it has formed.[40]

3.2 Microwave measurements

Due to fuel efficiency considerations, modern aircraft are forced to avoid metallic shields and solid radar absorbing materials. Instead, low radar reflection shielding enclosures are recommended with window apertures made of metallic knitted mesh, wire screens, or honeycombs.[41] Knitted screens, though a cost effective EM shielding solution, are likely to fail at high frequencies, since they exceed the waveguide's cut-off frequency. Vacuum deposited thin film wire materials can serve the purpose, but the skin effect begins to diminish their shielding effectiveness above 10 MHz. For this purpose, we believe that carbonaceous honeycombs are suitable since they are microporous, effectively consist of a series of tiny conducting waveguides assembled in parallel, and have stable shielding effectiveness up to the K_u band (12–18 GHz). Here we investigate pyrolysed cork, which resembles a rigid honeycomb like microstructure, as an effective lightweight candidate for broad band radar absorber applications.

As we expected, the un-pyrolysed cork samples were uniformly poor at absorbing over the X-band, with total shielding effectiveness (SE_T) values of only between −0.01 to −1.3 dB. Measurements were made on a variety of samples: MF5 cork powder, very fine cork dust (<100 μm diameter), solid cork (two samples, A and B), flat cork sheets and solid partially combusted cork (a commercial product, heated at 300 °C in air). All were equally poor in EM wave attenuation, as can be seen from the results in Table 1.

Measurements were also made on pyrolysed MF5 powder, mounted in a wax composite (20 wt% pyrolysed cork). This cork powder was very fine, and impossible to handle and fill in the wave guide without using a wax matrix. The sample was 1.65 mm thick. This had greatly improved absorption values in the X-band, as shown in Fig. 5, with SE_R = −4.2 to −7.9 dB, SE_A = −8.9 to −11.6 dB, and SE_T = −14.4 to −18.1 dB, over the X-band range of 8–12 GHz. This is a reasonably high SE_T value, especially for a sample only 1.65 mm thick, and one which only contains 20 wt% pyrolysed cork powder. It should be noted that although the trend and approximate value is clear from the plots, there is a small but consistent variation in SE_A due to the high level of porosity of these samples. Nevertheless, this does not affect the validity of these results, and we give the minimum and maximum values encountered for each sample.

Various pyrolysed solid cork samples were made with thicknesses of approximately 3, 5, 7 and 8.6 mm, and their shielding effectiveness values are shown in Table 2 and Fig. 6a–d. These were pure cork samples, with no wax matrix, and the materials could be easily handled and cut/ground to the desired shape. These samples gave much better SE_T values, which as expected, increased with thickness. The thinner

Table 1 Microwave absorption properties in the X-band (8–12 GHz) of un-pyrolysed cork samples

Cork type	Thickness (mm)	SE_R (dB)	SE_A (dB)	SE_T (dB)
MF5 cork powder	1.78	−0.1 to −1.2	−0.01 to −0.3	−0.2 to −1.3
Fine cork dust	1.60	−0.1 to −1.1	−0.01 to −0.2	−0.1 to −1.2
Solid cork A	5.70	−0.1 to −0.8	−0.01 to −0.4	−0.1 to −1.1
Solid cork B	5.90	−0.1 to −0.8	−0.01 to −0.4	−0.1 to −1.1
Flat cork sheet	5.75	0.1 to −0.2	−0.2 to −0.3	−0.3 to −0.6
Partially combusted cork	8.05	−0.01 to −0.7	−0.01 to −0.2	−0.01 to −0.2

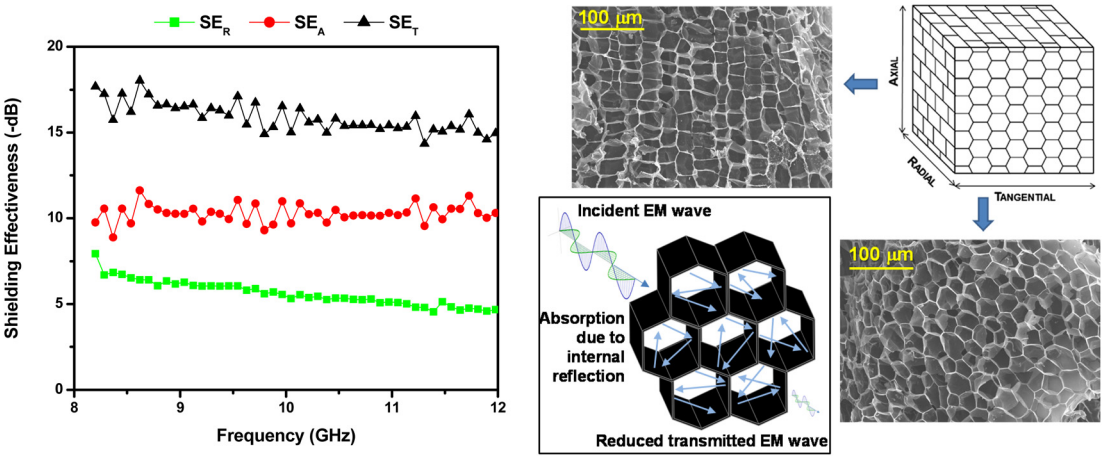

Fig. 5 X-band shielding effectiveness of pyrolysed cork powder (1.65 mm thick, 20 wt% mounted in wax matrix), and the suggested mechanism of enhanced absorption by internal reflection of the EM wave within the cork-carbon cells.

Table 2 Microwave absorption properties in the X-band (8–12 GHz) of pyrolysed solid cork samples

Thickness (mm)	SE_R (dB)	SE_A (dB)	SE_T (dB)
2.96	−3.7 to −8.7	−12.3 to −17.7	−19.8 to −23.3
4.98	−3.8 to −8.5	−14.1 to −18.5	−20.4 to −24.5
6.95	−3.8 to −7.4	−22.9 to −27.7	−28.5 to −32.7
8.60	−3.9 to −7.6	−27.5 to −34.0	−34.0 to −38.3

samples had good SE_T values of −19.8 to −23.3 dB for the 3 mm thick sample, and −20.4 dB to −24.5 dB for the 5 mm thick sample, while the 7 mm and 8.6 mm samples gave excellent SE_T values of −28.5 to −32.7 dB, and −34.0 to −38.3 dB, respectively. It is possible that the small nitrogen content that naturally occurs in this wood-derived carbon N doping could improve the MW absorption performance; however, the clear advantage of cork-derived carbon is its unique microstructure and light weight. These values compare very well with those reported for a PMMA (polymethyl methacrylate) composite with 7 wt% CNTs added, which gave an SE_T of −35 to −40 dB over the X-band,[28] although the cork material used here is much more simple and economic to produce, and more importantly, utilises a waste stream as the source. They also compare well to 3 mm thick carbon fibre/CNT/nickel powder composites, which had a SE_T of around −29 dB with just carbon fibre (61.3 wt% in a 38.7 wt% pyrolysed phenolic resin matrix), and around −45 to −48 dB with 1.9 wt% CNTs and 0.4 wt% Ni powder added.[26] Again, this composite would be a lot more complex and expensive to produce and contains a small amount of metal nickel particles. Epoxy matrix composites with 15 wt% graphene added only achieved an SE_T of around −21 dB over the X-band.[42]

It should also be noted that the reflection loss, SE_R, remains constant at between −4 to −8 dB whatever the thickness of the sample, while the absorption losses (SE_A) increase steadily with increasing sample thickness (see Table 2 and Fig. 6). This is because the cork honeycomb surface microstructure responsible for the reflection losses remains constant in all samples (and with the same electrical conductivity of the carbonaceous honeycomb structure), whereas the bulk of the material responsible for the absorption losses increases in depth with thickness, with a proportionate increase in internal reflecting from parallel hexagonal honeycombs. This confirms the suggestion by other authors working on carbon foams[43] that this is a consequence of more multiple reflections of the EM wave per unit volume within the cells of their 100 μm porous foam, attenuating radiated EM energy through the structure. In our case, this is occurring within the ultra-porous 20 μm honeycomb architecture of cork (Fig. 5), the volume of which increases with increasing thickness.

However, what is really unique about our pyrolysed cork absorbers is their ultra-low density, which gives them one of the highest specific shielding effectiveness (SSE) reported. As the density of the solid pyrolysed cork is only 0.031 g cm^{-3}, with no polymer matrix, binder or other material added, they have extremely high SSE values, as shown in Table 3 and Fig. 7. SSE increases with thickness, with little difference between the 3 and 5 mm samples, but then large increases as the thickness (and, hence, volume available for internal reflection/absorption) increases to 7 and 8.6 mm. These values range between −660 to −1235 dB g^{-1} cm^3, and the upper SSE values are more than twice those of any previously reported carbonaceous foams.

There are very high SSE values reported for aerogels created from the freeze drying of carbon or cellulose precursors, although these can be considered a different class of material to standard foams, and can reach incredibly low densities of <0.003 g cm^{-3} in some cases. However, the highest reported values for pure graphitic carbon aerogels are for carbonised cellulose fibre aerogels which had an SSE of 800 dB cm^3 g^{-1} (δ = 0.02 g cm^{-3}). These combined with reduced graphene oxide (RGO) attained SSE values of 6406 dB cm^3 g^{-1} (δ = 0.0047 g cm^{-3}) for 67% cellulose fibre/33% RGO aerogels annealed

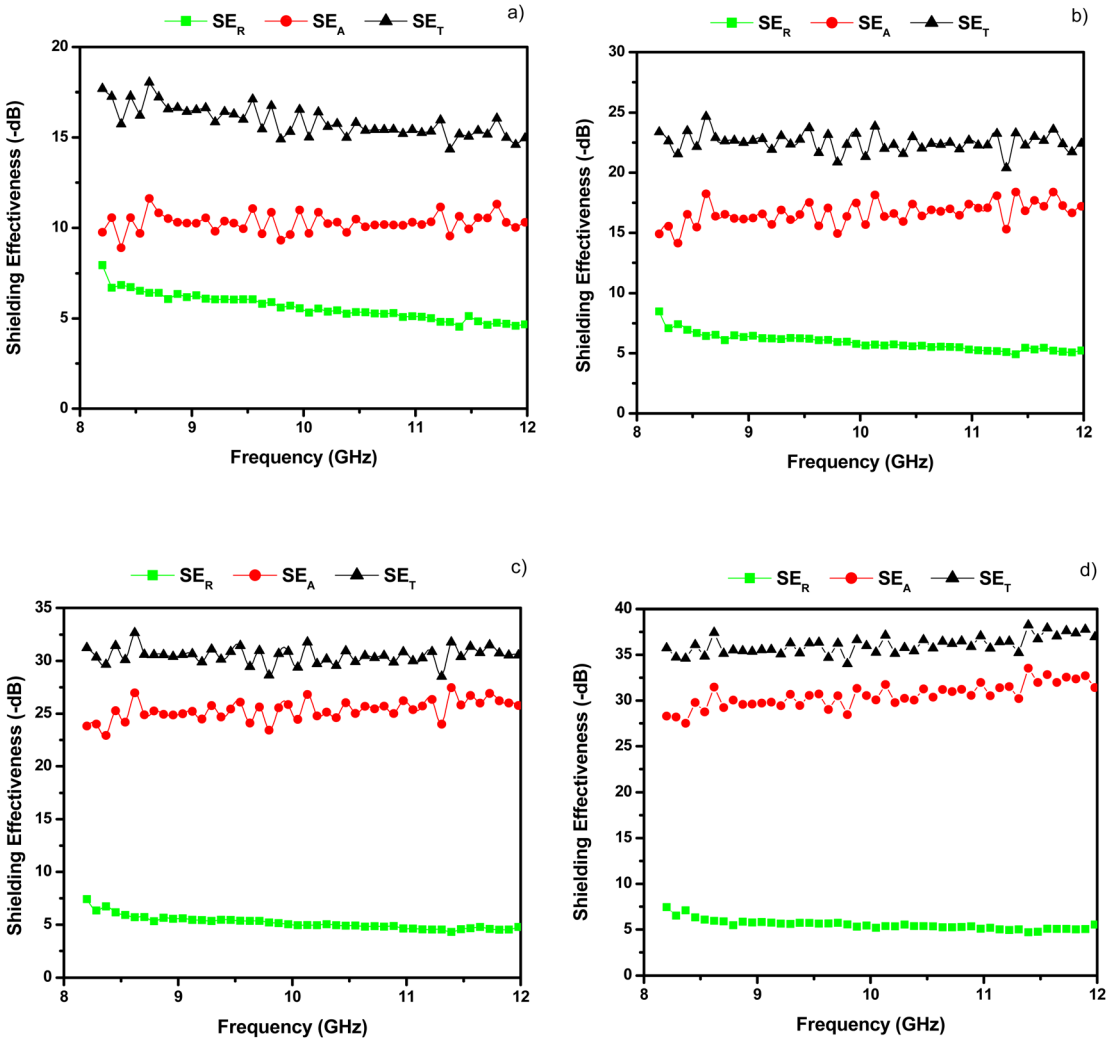

Fig. 6 X-band shielding effectiveness of pyrolysed solid cork for samples (a) 3 mm, (b) 5 mm, (c) 7 mm and (d) 8.6 mm thick.

Table 3 Specific shielding effectiveness (SSE) of pyrolysed solid cork samples in the X-band (8–12 GHz)

Thickness (mm)	SE_T (dB)	Density (g cm^{-3})	SSE (dB g^{-1} cm^3)
2.96	−19.8 to −23.3	0.031	−638.7 to −751.6
4.98	−20.4 to −24.5		−658.0 to −790.3
6.95	−28.5 to −32.7		−919.4 to −1054.8
8.60	−34.0 to −38.3		−1096.8 to −1235.5

under Ar/600 °C, and a SSE of 16 890 dB cm^3 g^{-1} (δ = 0.0028 g cm^{-3}) was reported for the same annealed under H_2 at 1000 °C.[44] Even more complex 3D porous aerogel structures made of 2D transition metal carbides (MXene) made by bidirectional freeze-casting have also been reported, with $Ti_3C_2T_x$ (T_x = the surface terminations) having an SSE of 8818 dB cm^3 g^{-1} (δ = 0.011 g cm^{-3}).[45] $Ti_3C_2T_x$ MXene@Ni microspheres have also recently been reported (measured over 2–18 GHz), exhibiting a superior minimum reflection loss value of −59.6

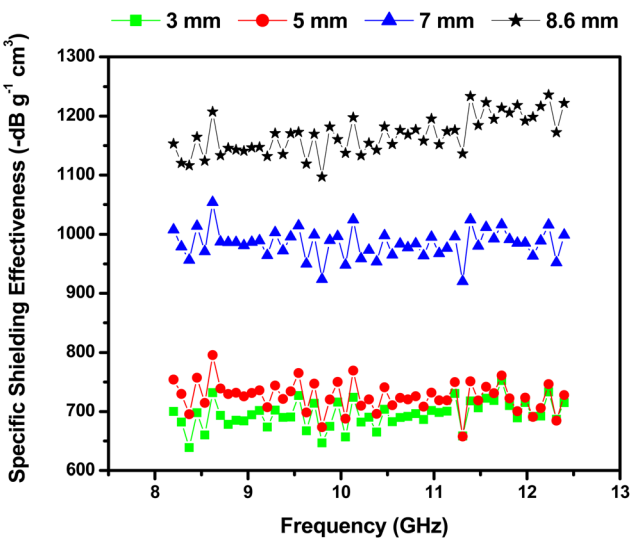

Fig. 7 Specific shielding effectiveness (SSE) of pyrolysed solid cork samples of various thicknesses in the X-band (8–12 GHz).

dB with a thickness of ~1.5 mm with an absorption bandwidth of 4.48 GHz around ~14 GHz, but no SSE values were given.[46] Honeycomb-like aerogels produced from freeze dried and carbonised lignin had an SSE of 533 dB cm^3 g^{-1} (δ = 0.03 g cm^{-3}), but when doped with 7.5 mg ml^{-1} RGO these aerogels obtained SSE values as high as 5750 dB cm^3 g^{-1} (δ = 0.0015 g cm^{-3}).[47] RGO additions were shown to reduced aerogel shrinkage and compression, but the SSE values for purely graphitic carbon aerogels are inferior to our cork-derived foams, and they had similar densities.

There have been many reports of carbon, graphite and graphene foams,[48] and interest in carbonaceous foams as light weight microwave absorbers. In 2004, carbon foams with 400–600 mm cells were made from petroleum mesophase pitch under high pressure at 450 °C, cut into 10 mm high sections, and mounted as filler in sandwich structures between carbon fibre reinforced composites (CFRC) and glass fibre reinforced composites (GFRC). There MW absorption was measured between 2–18 GHz, and in the X band the CFRC/foam sandwich had a SE_T of −5 to −10 dB, and in the CFRC/foam/GFRC sandwich SE_T = −8 to −15 dB.[49] The foam was never measured by itself, and no densities were given for the sandwiches, although they will have been >1 g cm^{-3}. Carbon foams with large cell sizes of 2–3 mm were made and measured over the X-band in 2006, with a stated relative density of 30%, which if graphite would equal ~0.68 g cm^{-3}.[50] The samples were 20 mm thick, and had SE_T = −8 to −12 dB, giving a rather low SSE of around −12 to −18 dB.

In 2005, polystyrene foams with 0.5–7 wt% CNTs added were measured over the X-band.[51] These authors did not state the density of their foam composites, but gave a SSE value of −33.1 dB g^{-1} cm^3 for the foam composite containing 7 wt% CNTs, which is clearly a rather low value. As these authors gave a SE_T value of −18.56 dB, we can infer that the density of this composite was in fact 0.56 g cm^{-3}. The foams they produced contained 40 to 170 μm cells, and the matrix contained a mass of CNTs which more resembled tangled spaghetti. Measurements showed that reflection from the CNTs, rather than absorption in the volume, was the dominant mechanism. No values were given for the thickness of these samples, but from the SEM image included, they appear to be around 1 mm thick. The density of the 20 wt% pyrolysed cork/wax composite used for our powder MW measurements was 0.95 g cm^{-3}, so this had similarly low SSE values to other composites.

PMMA/graphene nanocomposite microcellular foams (4 mm thick) were produced in 2011 with 0.5–5 wt% graphene, and these also had relatively high densities of 0.58–0.79 g cm^{-1}.[52] They contained closed, spherical cells under 10–20 μm in diameter, which became fewer, smaller and more irregular in shape with increasing graphene addition. The SE_T was −9.5 dB with 0.5 wt% graphene, and −20 dB with 1.8 wt%. Due to their relatively high densities, these foams only had SSE values of −14.6 and −25.3 dB g^{-1} cm^3, respectively. CNT reinforced carbon composite foams with interconnected cellular structure prepared by thermo-foaming molten sucrose followed by carbonization were reported in 2016.[53] The cells averaged 0.5–1.4 mm in diameter, and density varied from 0.14 g cm^{-3} for the foam with no CNTs added, to 0.24 g cm^{-3} when 2.5 wt% CNTs were included. The pure carbon foam (5 mm thick) had a SE_T of ~20 dB and SSE of −136 dB g^{-1} cm^3, while that with 2.5 wt% CNTs had a SE_T of ~39 dB and SSE of 166 dB g^{-1} cm^3.

Another paper in 2012 reported the absorption of commercial carbon foams between 1–4 GHz (not in the X-band).[54] The foams used were GRAFOAM® FPA-20 (0.324 g cm^{-3}) and GRAFOAM® FPA-10 (0.166 g cm^{-3}), with thicknesses between 1–4 mm. FPA-20 consisted of cells around 350 mm wide, and was a solid structure based on cells connected through open faces, mostly formed by regularly tetrahedral or tetrakaidecahedral unit cells. FPA-10 was a partly-open and partly-closed foam, consisting of randomly distributed spherical pores, ranging from 30–250 μm, connected by holes in their spherical cell walls. The 4 mm FPA-20 and 2 mm FPA-10 foams had good SE_T values between −30 to −50 dB over the 1–4 GHz range, and due to their lower densities, they had reasonable SSE values of −125 to −155 and −195 to −250 dB g^{-1} cm^3, respectively. Graphite foam made from coal tar pitch (200–300 μm cells) with iron NPs added as 10 wt% ferrocene was produced, with densities of 0.52 and 0.62 g cm^{-3} for the pure graphite foam and that with 10 wt% ferrocene, respectively. 2.7 mm thick samples had SE_T values of −35 to −39 dB and −75 to −81 dB, respectively, giving reasonable SSE values of −67 to −75 dB and −120 to −130 dB, respectively.[55]

There are several reports of extremely light-weight graphene foams, but none give data for MW measurements on the pure, unadulterated foam. Extremely lightweight graphene foams with 30–90 μm cells were reported in 2016, and had good SE_T values of −12 to −20 dB over the X-band with 10 mm thick samples. However, their MW absorption was measured on foam samples attached to an aluminium plate backing layer, greatly increasing both the EM reflection, and of course the overall weight of the measured sample.[56] Similarly, ultra lightweight graphene/CNT/Fe_3O_4 NP composite foams were reported as having SE_T values of −7 to −8 dB, −2 to −17 dB, and −4 to −33 dB over the X-band, for the pure graphene foam, graphene/NP foam and graphene/CNT/NP foam, respectively.[57] However, these samples were measured as wax composites, without details of their loading or weight. Therefore, as no values were published for any of these graphene based foams alone, no volume based SSE values published, or any densities given for the actual measured samples, we cannot compare them to our data here. Flexible, 1 mm thick foams of 0.8 wt% graphene in a poly(dimethyl siloxane) (PDMS) polymer matrix with a low density of 0.06 g cm^{-1} were reported in 2013, with SE_T of −20 to −30 dB, and SSE of −333 to −500 dB g^{-1} cm^3 over the X-band.[58]

The only paper with SSE results close to ours for a graphitic carbon foam was published in 2016, and details the creation of phenolic foams, carbonised at 450 °C in air, and with added CNTs and magnetic Fe_3O_4 nanoparticles (NPs).[59] The 3 mm thick foams were investigated with just CNTs added, and with CNTs and magnetite (ferrite) NPs added, and also for vari-

Table 4 Comparison of the microwave SSE values reported here with the best of those previously published for carbonaceous foams, over the whole X-band. Those highlighted are our pyrolysed cork samples

Material and thickness	Density (g cm^{-3})	SSE (dB g^{-1} cm^3)	Ref.
3 mm pyrolysed solid cork	0.031	−640 to −750	This paper
7 mm pyrolysed solid cork	0.031	−920 to −1055	This paper
8.6 mm pyrolysed solid cork	0.031	−1100 to −1235	This paper
5 mm carbonised cellulose fibre aerogel	0.020	−800	47
3.5 mm CVD CNT "sponge"	0.020	−1100	60
3 mm phenolic foam/2% CNTs/1% Fe_3O_4	0.127	∼−315	59
3 mm phenolic foam/2% CNTs/7% Fe_3O_4	0.126	∼−517	59
5 mm phenolic foam/2% CNTs/7% Fe_3O_4	0.126	∼−555	59
3 mm phenolic foam/1% CNTs	0.109	∼−185	59
3 mm phenolic foam/2% CNTs	0.110	∼−245	59
3 mm phenolic foam/5% CNTs	0.106	∼−330	59
3 mm phenolic carbon foam	0.104	∼−120	59
1 mm PDMS/0.8 wt% graphene	0.06	−33 to −500	58
2 mm FPA-10 graphite foam[a]	0.166	−195 to −250	54[a]
4 mm FPA-20 graphite foam[a]	0.324	−125 to −155	54[a]
5 mm pyrolysed sucrose foam	0.14	−136	53
5 mm pyrolysed sucrose foam/2.5% CNTs	0.24	−166	53
4 mm PMMA/0.5% graphene	0.58	−14.6	52
4 mm PMMA/5% graphene	0.79	−25.3	52
1 mm polystyrene/7% CNTs	0.56	−33.1	51
20 mm graphite foams	0.68	−12 to −18	50

[a] This material was measured at 1–4 GHz, not over the X-band.

ations in thickness between 0.5–5 mm for the best sample. The pure carbonised phenolic foam was rather poor, with SE_T between −11 to −13 dB over the X-band. This had a low density of 0.104 g cm^{-3}, giving it a reasonable SSE of ∼−120 dB g^{-1} cm^3. When between 1–5 wt% CNTs were added, SE_T increased considerably (up to −35 dB) with little change in density, giving SSE values of ∼−185, ∼−245 and ∼−330 dB g^{-1} cm^3, for 1 wt%, 2 wt% and 5 wt% CNTs added, respectively. When the ferrite NPs were added to the foam with 2 wt% CNTs, even better results were obtained, despite a greater increase in density of up to 0.130 g cm^{-3}. This gave SE_T values between ∼−35 dB with 1 wt% NPs, and ∼−62 dB with 7 wt% NPs added, resulting in high SSE values of ∼−315 and ∼−517 dB g^{-1} cm^3, respectively. When the thickness of the foam with 2 wt% CNTs and 7 wt% NPs was increased to 5 mm, an even higher SE_T of ∼−70 dB and SSE of ∼−555 dB was achieved. The other work which achieved values similar to ours was for CNT "sponges", which in fact resembled more CNT mats, made from a complicated process of chemical vapour deposition (CVD) at 860 °C with ferrocene and 1,2-dichlorobenzene under Ar/H_2 gas.[60] This produced very lightweight carbon materials 2–3.5 mm thick, with a density of only 0.02 g cm^{-3}. These had very good SE values of between −12 to −24 dB across the X-band for samples 1.5–3 mm thick, and due to their low density they achieved SSE values as high as 1100 dB cm^3 g^{-1}, comparable to our cork-derived foams.

As discussed above, our results achieve more than double the graphitic foams with 2 wt% CNTs and 7 wt% NPs above, are superior to pure graphitic carbon aerogels, and are as good as the ultra-light-weight CNT "sponge". We do this with a simple, natural and fully renewable waste material, exploiting its inherent porous microstructure, formed of (amorphous) graphitic carbon, and with no added matrix, binder, pore forming/blowing agents, or added CNTS, graphene, metals or NPs. We achieve this because of the extraordinarily low density of the pyrolysed cork, and its intact and periodic honeycomb microstructure that enables internal reflection based EM wave attenuation capabilities. Some of our results are summarised and compared to those previously published, in Table 4. For samples of the same thickness (3 mm), our pyrolysed solid cork sample has a SSE 1.5 times greater than graphene/PDMS foams, and is 6 times greater than the best pure carbon graphitic foam previously reported with no additives (*e.g.*, CNTs, NPs) in the X-band. It is also 3 times greater than the values measured for the commercial GRAFOAM® FPA-10 graphite foam between 1–4 GHz.

4. Conclusions

Pyrolysed cork was investigated for the first time as an ultra-light-weight MW absorbing material and potential RAM /EMI shield in the X-band (8–12 GHz). Although cork is already a remarkably light weight material, the pyrolysed cork was ultra-light-weight, with a density of only 0.031 g cm^{-3} due to its naturally porous honeycomb structure. It was shown to be made of amorphous/mesoporous carbon. Although pyrolysed cork powder had a reasonable SE_T of −14.4 to −18.1 dB over the X-band, the advantage of its low density was lost as it was mixed as 20 wt% in a wax composite for measurement. However, solid pyrolysed cork cold be cut and polished to precise shape, and so maintained its ultra-low density. Multiple internal reflection effects emanating from the regularly arranged honeycomb microstructure of pyrolysed cork

were found to be ideal for EM wave absorption through scattering losses. Not only did it have excellent SE_T values of between −19.8 to −23.3 dB when 3 mm thick, up to −34.0 to −38.3 dB when 8.6 mm thick, over the X-band, but we also achieved one of the highest ever reported MW specific shielding effectiveness (SSE) values. These ranged from −640 to −1235 dB g^{-1} cm^3, depending on thickness, the upper value being more than twice that of any previously reported carbonaceous foams. For samples 3 mm thick, our pyrolysed solid cork sample has a SSE 1.35 times greater than the highest previously reported material which was a carbon foam/CNT/NP mix, 6 times greater than the best pure graphitic carbon foam over the X-band, and 3 times greater than commercial graphite foams measured between 1–4 GHz. It should be noted that cork is a sustainable and totally renewable material, which is much more simple and economic to produce than the composites and foams reported previously, and we valorised a waste stream as the source for our cork.

Conflicts of interest

There are no conflicts to declare.

Acknowledgements

This work was developed within the scope of the project CICECO-Aveiro Institute of Materials, UIDB/50011/2020 & UIDP/50011/2020, financed by national funds through the FCT/MEC and when appropriate co-financed by FEDER under the PT2020 Partnership Agreement. R. C. Pullar wishes to thank FCT grant IF/00681/2015 for supporting this work. R. M. Novais wishes to thank FCT project H2CORK (PTDC/CTM-ENE/6762/2014) and FCT grant CEECIND/00335/2017. A. P. F. Caetano thanks FCT project "Bio4MURAL" PTDC/HAR-ARQ/29157/2017. K. P. Surendran and R. C. Pullar wish to acknowledge the FCT-DST Indo-Portuguese bilateral project (INT/Portugal/P-09/2013) for supporting this work.

References

1 APCOR, Yearbook 2016. Portuguese Cork Association (Portugal), 2016. Available from: https://www.apcor.pt/en/portfolio-posts/apcor-year-book-2016/. Accessed June 2023.
2 A. M. Matos, S. Nunes and J. Sousa-Coutinho, Cork waste in cement based materials, *Mater. Des.*, 2015, **85**, 230–239.
3 O. Anjos, C. Rodrigues, J. Morais and H. Pereira, Effect of density on the compression behavior of cork, *Mater. Des.*, 2014, **53**, 1089–1096.
4 https://www.saomarcosdaserra.com/cork.php. Accessed June 2023.
5 L. Gil, Cork: a strategic material, *Front. Chem.*, 2014, **2**, 16.
6 E. M. Fernandes, V. M. Correlo, J. F. Mano and R. L. Reis, Cork-polymer biocomposites: mechanical, structural and thermal properties, *Mater. Des.*, 2015, **82**, 282–289.
7 O. Anjos, H. Pereira and M. E. Rosa, Tensile properties of cork in the tangential direction: variation with quality, porosity, density and radial position in the cork plank, *Mater. Des.*, 2010, **31**, 2085–2090.
8 S. P. Silva, M. A. Sabino, E. M. Fernandes, V. M. Correlo, L. F. Boesel and R. L. Reis, Cork: properties, capabilities and applications, *Int. Mater. Rev.*, 2008, **53**, 345–365.
9 https://www.engineeringtoolbox.com/wood-density-d_40.html. Accessed June 2023.
10 M. I. Fletcher, Balsa: Production and Utilization, *Econ. Bot.*, 1951, **5**, 107–125.
11 https://www.corkqc.com/pages/industry-statistics. Accessed June 2023.
12 https://www.apcor.pt/en/cork/recycling. Accessed June 2023.
13 E. Atanes, A. Nieto-Márquez, A. Cambra, M. C. Ruiz-Pérez and F. Fernández-Martínez, Adsorption of SO_2 onto waste cork powder-derived activated carbons, *Chem. Eng. J.*, 2012, **211–212**, 60–67.
14 B. Cardoso, A. S. Mestre, A. P. Carvalho and J. Pires, Activated carbon derived from cork powder waste by KOH activation: preparation, characterization, and VOCs adsorption, *Ind. Eng. Chem. Res.*, 2008, **47**, 5841–5846.
15 M. Demertzi, J. A. Paulo, L. Arroja and A. C. Dias, A carbon footprint simulation model for the cork oak sector, *Sci. Total Environ.*, 2016, **566–567**, 499–511.
16 I. Cabrita, B. Ruiz, A. S. Mestre, I. M. Fonseca, A. P. Carvalho and C. O. Ania, Removal of an analgesic using activated carbons prepared from urban and industrial residues, *Chem. Eng. J.*, 2010, **163**, 249–255.
17 A. M. A. Pintor, C. I. A. Ferreira, J. C. Pereira, P. Correia, S. P. Silva, V. J. P. Vilar, C. M. S. Botelho and R. A. R. Boaventura, Use of cork powder and granules for the adsorption of pollutants: a review, *Water Res.*, 2012, **46**, 3152–3166.
18 R. C. Pullar, P. Marques, J. Amaral and J. A. Labrincha, Magnetic wood-based biomorphic $Sr_3Co_2Fe_{24}O_{41}$ Z-type hexaferrite ecoceramics made from cork templates, *Mater. Des.*, 2015, **82**, 297–303.
19 R. C. Pullar and R. M. Novais, Ecoceramics - Cork-based Biomimetic Ceramic 3-DOM Foams, *Mater. Today*, 2017, **20**, 45–46.
20 F. C. Oliveira, M. Alexandra Barreiros, S. Abanades, A. P. F. Caetano, R. M. Novais and R. C. Pullar, Solar thermochemical CO_2 splitting using cork-templated ceria ecoceramics, *J. CO_2 Util.*, 2018, **26**, 552–563.
21 R. M. Novais, A. P. F. Caetano, M. P. Seabra, J. A. Labrincha and R. C. Pullar, Extremely fast and efficient methylene blue adsorption using eco-friendly cork and paper waste-based activated carbon adsorbents, *J. Cleaner Prod.*, 2018, **137**, 1137–1147.
22 F. Qin and C. Brosseau, A review and analysis of microwave absorption in polymer composites filled with carbonaceous particles, *J. Appl. Phys.*, 2012, **111**, 061301.
23 G.-S. Wang, X.-J. Zhang, Y.-Z. Wei, S. He, L. Guo and M.-S. Cao, Polymer composites with enhanced wave absorp-

tion properties based on modified graphite and polyvinylidene fluoride, *J. Mater. Chem. A*, 2013, **1**, 7031–7036.
24 K. H. Wu, T. H. Ting, G. P. Wang, W. D. Ho and C. C. Shih, Effect of carbon black content on electrical and microwave absorbing properties of polyaniline/carbon black nanocomposites, *Polym. Degrad. Stab.*, 2008, **93**, 483–488.
25 W. Liu, S. Tan, Z. Yang and G. Ji, Hollow graphite spheres embedded in porous amorphous carbon matrices as lightweight and low-frequency microwave absorbing material through modulating dielectric loss, *Carbon*, 2018, **138**, 143–153.
26 X. Liu, X. Yin, L. Kong, Q. Li, Y. Liu, W. Duan, L. Zhang and L. Cheng, Fabrication and electromagnetic interference shielding effectiveness of carbon nanotube reinforced carbon fiber/pyrolytic carbon composites, *Carbon*, 2014, **68**, 501–510.
27 A. Saib, L. Bednarz, R. Daussin, C. Bailly, X. Lou, J.-M. Thomassin, C. Pagnoulle, C. Detrembleur, R. Jérôme and I. Huynen, Carbon Nanotube Composites for Broadband Microwave Absorbing Materials, *IEEE Trans. Microwave Theory Tech.*, 2006, **54**, 2745–2754.
28 S. Pande, B. P. Singh, R. B. Mathur, T. L. Dhami, P. Saini and S. K. Dhawan, Improved Electromagnetic Interference Shielding Properties of MWCNT–PMMA Composites Using Layered Structures, *Nanoscale Res. Lett.*, 2009, **4**, 327–334.
29 H. Yu, T. Wang, B. Wen, M. Lu, Z. Xu, C. Zhu, Y. Chen, X. Xue, C. Sun and M. Cao, Graphene/polyaniline nanorod arrays: synthesis and excellent electromagnetic absorption properties, *J. Mater. Chem.*, 2012, **22**, 21679–21685.
30 C. Wang, X. Han, P. Xu, X. Zhang, Y. Du, S. Hu, J. Wang and X. Wang, The electromagnetic property of chemically reduced graphene oxide and its application as microwave absorbing material, *Appl. Phys. Lett.*, 2011, **98**, 072906, DOI: 10.1063/1.3555436.
31 MF5 cork granules, specification sheet PDA 1023/9, Amorim Cork Composites.
32 K. Krishnamoorthy, M. Veerapandian, R. Mohan and S. Kim, Investigation of Raman and photoluminescence studies of reduced graphene oxide sheets, *Appl. Phys. A: Mater. Sci. Process.*, 2012, **106**, 501–506.
33 M. Marton, M. Vojs, E. Zdravecká, M. Himmerlich, T. Haensel, S. Krischok, M. Kotlár, P. Michniak, M. Veselý and R. Redhammer, Raman Spectroscopy of Amorphous Carbon Prepared by Pulsed Arc Discharge in Various Gas Mixtures, *J. Spectrosc.*, 2013, **2013**, 467079.
34 S. Perumbilavil, P. Sankar, T. P. Rose and R. Philip, White light Z-scan measurements of ultrafast optical nonlinearity in reduced graphene oxide nanosheets in the 400–700 nm region, *Appl. Phys. Lett.*, 2015, **107**, 051104.
35 F. Tuinstra and J. L. Koenig, Raman Spectrum of Graphite, *J. Chem. Phys.*, 1970, **53**, 1126–1130.
36 J.-G. Li, C.-Y. Tsai and S.-W. Kuo, Fabrication and Characterization of Inorganic Silver and Palladium Nanostructures within Hexagonal Cylindrical Channels of Mesoporous Carbon, *Polymers*, 2014, **6**, 1794–1809.
37 F. Vasileios, P. Ioannis, S. Nikolaos, E. Ioannis and T. Kostas, Analysis of logging forest residues as an energy source, (2018). Analysis of logging forest residues as an energy source, *J. Agric. Informatics*, 2018, **9**, 431.
38 R. M. Novais, M. Saeli, A. P. F. Caetano, M. P. Seabra, J. A. Labrincha, K. P. Surendran and R. C. Pullar, *Constr. Build. Mater.*, 2019, **229**, 116930.
39 P. Serp, *Comprehensive Inorganic Chemistry II - (Second Edition), Volume 7: From Elements to Applications, Chapter 7.13 – Carbon*, 2013, pp. 323–369.
40 R. H. Telling, C. P. Ewels, A. A. El-Barbary and M. I. Heggie, Wigner defects bridge the graphite gap, *Nat. Mater.*, 2003, **2**, 333–337.
41 X. C. Tong, *Advanced Materials and Design for Electromagnetic Interference Shielding*, CRC Press, Taylor & Francis Group, Boca Raton, USA, 2009.
42 J. Liang, Y. Wang, Y. Huang, Y. Ma, Z. Liu, J. Cai, C. Zhang, H. Gao and Y. Chen, Electromagnetic interference shielding of graphene/epoxy composites, *Carbon*, 2009, **47**, 922–925.
43 Q. Li, L. Chen, J. Ding, J. Zhang, X. Li, K. Zheng, X. Zhang and X. Tian, Open-cell phenolic carbon foam and electromagnetic interference shielding properties, *Carbon*, 2016, **104**, 90–105.
44 Y.-J. Wan, P.-L. Zhu, S.-H. Yu, R. Sun, C.-P. Wong and W.-H. Liao, Ultralight, super-elastic and volume-preserving cellulose fiber/graphene aerogel for high-performance electromagnetic interference shielding, *Carbon*, 2017, **115**, 629–639.
45 M. Han, X. Yin, K. Hantanasirisakul, X. Li, A. Iqbal, C. B. Hatter, B. Anasori, C. M. Koo, T. Torita, Y. Soda, L. Zhang, L. Cheng and Y. Gogotsi, Anisotropic MXene Aerogels with a Mechanically Tunable Ratio of Electromagnetic Wave Reflection to Absorption, *Adv. Opt. Mater.*, 2019, **2019**, 1900267.
46 C. Wen, X. Li, R. Zhang, C. Xu, W. You, Z. Liu, B. Zhao and R. Che, High-Density Anisotropy Magnetism Enhanced Microwave Absorption Performance in $Ti_3C_2T_x$ MXene@Ni Microspheres, *ACS Nano*, 2022, **16**, 1150–1159.
47 Z. Zeng, Y. Zhang, X. Y. D. Ma, S. I. S. Shahabadi, B. Che, P. Wang and X. Lu, Biomass-based honeycomb-like architectures for preparation of robust carbon foams with high electromagnetic interference shielding performance, *Carbon*, 2018, **140**, 227–236.
48 M. Inagaki, J. Qiu and Q. Guo, Carbon foam: Preparation and application, *Carbon*, 2015, **87**, 128–152.
49 J. Yang, Z. Shen and Z. Hao, Microwave characteristics of sandwich composites with mesophase pitch carbon foams as core, *Carbon*, 2004, **42**, 1882–1885.
50 Z. Fang, X. Cao, C. Li, H. Zhang, J. Zhang and H. Zhang, Investigation of carbon foams as microwave absorber: Numerical prediction and experimental validation, *Carbon*, 2006, **44**, 3348–3378.
51 Y. L. Yang and M. C. Gupta, Novel carbon nanotube-polystyrene foam composites for electromagnetic interference shielding, *Nano Lett.*, 2005, **5**(11), 2131–2134.
52 H. B. Zhang, Q. Yan, W. G. Zheng, Z. X. He and Z. Z. Yu, Tough graphene-polymer microcellular foams for electro-

magnetic interference shielding, *ACS Appl. Mater. Interfaces*, 2011, **3**, 918–924.

53 R. Narasimman, S. Vijayan, K. S. Dijith, K. P. Surendran and K. Prabhakaran, Carbon composite foams with improved strength and electromagnetic absorption from sucrose and multi-walled carbon nanotube, *Mater. Chem. Phys.*, 2016, **181**, 538–548.

54 F. Moglie, D. Micheli, S. Laurenzi, M. Marchetti and V. Mariani Primiani, Electromagnetic shielding performance of carbon foams, *Carbon*, 2012, **50**, 1972–1980.

55 R. Kumar, S. R. Dhakate, P. Saini and R. B. Mathur, Improved electromagnetic interference shielding effectiveness of light weight carbon foam by ferrocene accumulation, *RSC Adv.*, 2013, **3**, 4145–4151.

56 H. Chen, Z. Huang, Y. Yang, P. Xiao, Y. Zhou, Y. Chen, Y. Zhang and Y. Huang, Composition and structure control of ultralight graphene foam for high-performance microwave absorption, *Carbon*, 2016, **105**, 438–447.

57 L. Shi, Y. Zhao, Y. Li, X. Han and T. Zhang, Octahedron Fe3O4 particles supported on 3D MWCNT/graphene foam: In situ method and application as a comprehensive microwave absorption material, *Appl. Surf. Sci.*, 2017, **416**, 329–337.

58 Z. Chen, C. Xu, C. Ma, W. Ren and H. Cheng, Lightweight and Flexible Graphene Foam Composites for High–Performance Electromagnetic Interference Shielding, *Adv. Mater.*, 2013, **25**, 1296–1300.

59 Q. Li, L. Chen, J. Ding, J. Zhang, X. Li, K. Zheng, X. Zhang and X. Tian, Open-cell phenolic carbon foam and electromagnetic interference shielding properties, *Carbon*, 2016, **104**, 90–105.

60 M. Crespo, M. González, A. L. Elías, L. P. Rajukumar, J. Baselga, M. Terrones and J. Pozuelo, Ultra–light carbon nanotube sponge as an efficient electromagnetic shielding material in the GHz range, *Phys. Status Solidi RRL*, 2014, **8**, 698–704.